Pergamon

Geochimica et Cosmochimica Acta, Vol. 68, No. 7, pp. 3587–3597, 2004

0016-7037/04 $30.00 + .00

doi:10.1016/j.gca.2004.02.021

Heterogeneous bubble nucleation on Fe-Ti oxide crystals in high-silica rhyolitic melts

JAMES E. GARDNER[1,*] and MARIE-HÉLÈNE DENIS[2]

[1]Geophysical Institute and Department of Geology and Geophysics University of Alaska Fairbanks, Fairbanks, AK 99775-7320, USA
[2]Institut de Physique du Globe à Paris, 4 place Jussieu, 75252 Paris cedex 05, France

(*Received July* 8, 2003; *accepted in revised form February* 23, 2004)

Abstract—The nucleation of H_2O bubbles in magmas has been proposed as a trigger for volcanic eruptions. To determine how bubbles nucleate heterogeneously in silicate melts, experiments were carried out in which high-silica rhyolitic melts were hydrated at 740–800°C and 50–175 MPa, decompressed by 20–70 MPa, and held at the lower pressures for ≥10 s before being quenched. The hydration conditions were subliquidus, and all samples contain blocky magnetite + needle-shaped hematite ± plagioclase. Magnetite is abundant at 800°C and high pressures, whereas hematite becomes more abundant at lower temperatures and pressures. Bubbles nucleated in a single event in all samples, with the number density (N_T) of bubbles varying between 2×10^7 and 1×10^9 cm^{-3}. At low degrees of supersaturation, one to a few bubbles nucleate on faces of magnetite, but at medium to high degrees of supersaturation, multiple bubbles nucleate on single magnetite grains. On hematite, one to a few bubbles nucleated at the ends of the needle-shaped crystals at medium supersaturations, but formed along their entire lengths at high supersaturations. N_T increases as water diffusivity decreases, indicating that the number of bubbles nucleated is influenced by their growth, which depletes the melt with respect to H_2O and lowers supersaturation. If volcanic eruptions are triggered by bubble formation in magmas stored in shallow-level magma chambers, then the supersaturations needed for heterogeneous nucleation suggest that only small amounts of crystallization are needed, whereas homogeneous nucleation is unlikely to trigger eruptions.

1. INTRODUCTION

When magma ascends towards the surface it supersaturates with H_2O because of the lower pressure. That supersaturation induces bubbles to nucleate, and their subsequent growth can drive volcanic eruptions (e.g., Sparks, 1978). Stagnant magma may also nucleate bubbles, because it can supersaturate with H_2O as it crystallizes. Creating a gas phase in magma may actually trigger magma to erupt (Blake, 1984; Tait et al., 1989; Pyle and Pyle, 1995). Knowing the timing and rate of bubble nucleation is thus critical in modeling volcanic eruptions.

Classical nucleation theory predicts that the activation energy needed to nucleate bubbles homogeneously in silicate melts, resulting from random fluctuations of dissolved volatiles, is

$$\Delta F = \frac{16\pi\sigma^3}{3\Delta P^2} \tag{1}$$

where ΔF is the Helmholtz free energy for the formation of a critically sized nucleus, σ is surface tension (N m^{-1}), and ΔP is the supersaturation pressure (Navon and Lyakhovsky, 1998). Estimates for σ vary with melt composition, temperature, and dissolved H_2O contents, and range from ~0.06 to ~0.3 N m^{-1} in rhyolitic melt (Epel'baum et al., 1973; Bagdassarov et al., 2000; Mangan and Sisson, 2000). Dissolved H_2O contents especially appear to change σ, from ~0.27 N m^{-1} at "dry" conditions to 0.065 N m^{-1} at 400 MPa saturation (Bagdassarov et al., 2000). Because σ dominates the activation energy, values of ΔP needed for homogeneous nucleation varies, mainly with dissolved H_2O content: ~4–5 wt% H_2O requires ΔP on order of 120–310 MPa, whereas ~7–8 wt% requires ΔP of ~60–160 MPa (Hurwitz and Navon, 1994; Mourtada-Bonnefoi and Laporte, 1999, 2002; Mangan and Sisson, 2000).

If silicate melts contain heterogeneities, such as crystals, bubbles may nucleate more easily, because of a reduced σ (Hurwitz and Navon, 1994; Lasaga, 1998; Navon and Lyakhovsky, 1998). In this case, σ is a balance of surface tensions between the three phases: melt, bubble, and crystal (Hurwitz and Navon, 1994; Lasaga, 1998). Assuming a spherical bubble partially wets a flat crystal surface, the activation energy for nucleation becomes

$$\Delta F = \frac{16\pi\sigma^3}{3\Delta P^2}\phi\,, \tag{2}$$

where ΔF is changed by a factor ϕ, which is defined as

$$\phi = \frac{(2 - \cos\theta)(1 + \cos\theta)^2}{4}\,, \tag{3}$$

in which θ is the wetting angle between the bubble and crystal, and equals the balance of surface tensions

$$\cos\theta = \frac{(\sigma_{cv} - \sigma_{cm})}{\sigma_{mv}}\,, \tag{4}$$

where σ_{ij} is σ between two of the phases, crystal (c), bubble (v), or melt (m). Hurwitz and Navon (1994) found that magnetite in rhyolitic melts may reduce ΔP to ~1 MPa. The efficiency of nucleation on magnetite also increased as ΔP increased, with bubbles nucleating at ΔP <5 MPa on 50–60% of the magnetites present, but on >90% of them when ΔP >30 MPa. Nucleation on other crystal types differed, however, with ΔP ≥30 MPa needed to nucleate bubbles on biotite and ΔP

* Author to whom correspondence should be addressed, at Department of Geological Sciences, The University of Texas at Austin, Austin, TX 78712-0254, USA (gardner@mail.utexas.edu).

Table 1. Composition of starting material.[a]

SiO_2	75.2
Al_2O_3	14.5
FeO	0.1
MgO	0.7
CaO	1.1
Na_2O	3.8
K_2O	4.5

[a] Glass analysis by electron microprobe, normalized to 100%; oxides are in wt% (J. Larsen, personal communication).

= 30–50 MPa required for seeding on zircon. In contrast, bubbles did not nucleate on plagioclase up to supersaturations of 135 MPa. Hurwitz and Navon (1994) were unable to measure θ, and could thus only propose that differing nucleation on crystals resulted from variable surface roughness, which changes the geometric factor ϕ.

Bubble nucleation can be mitigated by growth of bubble nuclei, because their growth lowers the H_2O content, and thus ΔP, of the melt (Toramaru, 1989, 1995). Toramaru (1995) recognized that both melt viscosity or water diffusivity can play crucial roles, with higher viscosity or slower diffusion hindering bubble growth, and allowing for greater nucleation. Although bubble growth in silicate melts has been studied experimentally (Navon et al., 1998; Gardner et al., 1999, 2000; Liu and Zhang, 2000; Martel and Bureau, 2001) and sophisticated models now exist (Proussevitch et al., 1993; Navon et al., 1998; Proussevitch and Sahagian, 1998), there has been little work on heterogeneous nucleation of bubbles in silicate melts. Thus, here we examine heterogeneous nucleation of H_2O bubbles in a rhyolitic melt to investigate the influence of crystal types, water diffusion, and melt viscosity on heterogeneous nucleation.

2. EXPERIMENTAL AND ANALYTICAL METHODS

All experiments used fresh obsidian (MCR) from Mono Craters, California, which consists of clear, high-silica rhyolitic glass containing less than 1 vol% microlites of Fe-Ti oxides and plagioclase (Table 1). Pieces of obsidian were hand crushed and sieved, and powder between 45 and 90 μm in size was used in the experiments. All experiments were run in 4-mm-diameter (3.8 mm i.d.) Au capsules. First, one end of a capsule was welded shut with an oxy-acetylene torch. De-ionized water (~4 mg) and 40 to 60 mg of powder were then added to the capsule. The amount of water added was such that each charge contained, depending on run pressure, 6 to 10 wt% total water, which was enough to ensure the presence of excess vapor. The water wetted the powder before the run, filling void spaces between powder grains. The water-saturated powders were compacted in the capsules with a glass rod. A sample typically occupied a quarter of the capsule volume so it could expand during decompression. The open end was then welded shut. Capsules were weighed before and after sealing to verify that no water was lost.

Experiments were run in externally heated, cold-seal pressure vessels made of a Nickel-based alloy and fitted with rapid-quench extensions. The pressurizing medium was water, and a pressure transducer measured pressure to ±0.1 MPa. Temperature was monitored by K-type (chromel-alumel) thermocouples, precise to ±5°C. The sample holders are made of Inconel metal, which we found does not react with the pressurizing fluid, and thus oxygen fugacity was not buffered at the Ni-NiO oxygen buffer as when a Ni filler rod is used (Geschwind and Rutherford, 1992; Gardner et al., 1995). As shown below, almost all runs grew magnetite and hematite, and thus oxygen fugacity of our experiments equaled the magnetite-hematite buffer at the experimental run temperatures.

An experimental run consisted of three steps: hydration, decompression, and quench (Table 2). First, samples were equilibrated for 3 d at between 50 and 175 MPa and 740°, 775°, or 800°C. Next, pressure was reduced 20 to 70 MPa instantaneously by either opening the vessel to the pressure line that was set at a lower pressure or using a hand-operated intensifier installed on the pressure line. Only experiments hydrated at 50 MPa decompressed by opening the vessel to the line, in which pressure dropped in 1–2 s. All other runs were decompressed with the intensifier, by which pressure dropped in 2–4 s. Runs were then held at the new pressure for 10 to 21,600 s, with all times reported being times held after pressure had dropped (Table 2). Samples were then quenched by dropping the charge into a water-cooled chamber at the base of the pressure vessel. Quench rates are on order of 150°C s^{-1} (Dobson et al., 1989). Two runs were quenched without being decompressed. Capsules were removed from the vessels, checked to verify they had remained sealed, opened, and the samples were polished for bubble measurements.

The diameters of 100 to 250 bubbles were measured in each sample (Table 2), using the internal scale bar of a petrographic microscope (readable to ±0.5 μm). Only when the three-dimensional diameter of the nucleated bubbles could be seen were they measured. Bubble sizes do not vary between areas in a sample. For some samples, back-scattered-electron images or reflected-light images were taken using, respectively, scanning electron microscopy (SEM) or the petrographic microscope. Each image was digitized and analyzed using image analysis techniques to determine the area percentage of bubbles, which is assumed to equal volume percentage (porosity) (Table 2). Similar techniques were used to determine crystal contents of a few samples.

The number density of bubbles (N_T) was calculated from the relationship developed by Gardner et al. (1999):

$$N_T = \frac{\phi_M}{\sum_i \left(\frac{n_i}{N_M} V_i \right)} \quad (5)$$

where N_M is the number of bubbles measured in a sample, n_i is the number of bubbles of diameter i, V_i is the volume of a bubble of diameter i, and ϕ_M is the volume fraction of bubbles in a sample (porosity divided by 100). N_T is thus calculated from the porosity and measured size distribution of bubbles in a sample (Table 2). Errors for N_T, based on replicated measurements of porosities and bubble sizes in samples, are listed in Table 2. For a few samples, porosity was determined from only one image, and so an error on the corresponding N_T was not propagated. Crystal number densities in a few of the crystal-poor samples (Table 2) were determined using image analysis from back-scattered-electron images, following the methods of Sato (1995) and Gray (1970).

3. EXPERIMENTAL RESULTS

3.1. Starting Conditions and Crystals in the Experimental Runs

A few experiments were quenched without decompressing to establish the starting conditions of samples for nucleation. In all nondecompressed samples, there is a population of bubbles that are 20–70 μm in diameter, which we term hydration bubbles (Fig. 1). Those bubbles were originally spaces between powder grains that had filled with water during sample preparation. Assuming that the upper 75% of the capsule contained air of a standard density of 1225 g cm^{-3} (COESA, 1976) (neglecting humidity), we estimate that the mole fraction of H_2O in the fluid of each experiment was 0.9–0.95. Gardner et al. (1999) found that similar amounts of air has essentially no influence on water saturation in rhyolite melt. We have also found that when hydration bubbles are present H_2O saturation of MCR rhyolite

Table 2. Experimental conditions and results.[a]

Run	T (°C)	P_I (MPa)	P_F (MPa)	Time (s)	Size (μm)	Porosity (vol%)	BND[b] ($\times 10^8$ cm^{-3})	CND ($\times 10^6$ cm^{-3})
MC-31	800	175	175	—	—	—	—	0.05
MC-49	800	175	145	15	5	0.11	0.343 (9)	0.05
MC-51	800	150	125	15	3	0.07	0.270 (36)	0.03
MC-50	800	150	125	30	5	0.10	0.270 (81)	0.05
G-291	800	150	100	10	8	2.91	0.757 (255)	n.d.
G-299	800	150	100	35	4	3.00	0.719 (239)	n.d.
G-304	800	150	100	10	3	1.70	0.924 (392)	n.d.
G-307	800	150	100	25	3	1.56	0.616 (226)	n.d.
G-314	800	150	100	15	6	n.d.	n.d.	n.d.
G-305	800	150	80	25	7	3.49	1.17 (43)	n.d.
G-309	800	150	80	10	7	4.40	2.96 (14)	n.d.
G-310	800	150	80	25	6	3.59	1.80 (75)	n.d.
G-319	800	150	80	15	8	n.d.	n.d.	n.d.
G-324	800	150	80	17	5	n.d.	n.d.	n.d.
G-278	800	125	105	60	6	0.15	0.345	0.09
G-279	800	125	105	180	4	0.13	0.414	0.21
G-280	800	125	105	30	4	0.14	0.422	0.05
G-281	800	125	105	45	6	0.10	0.267	0.03
G-282	800	125	105	15	4	0.11	0.383	0.47
G-283	800	125	105	120	4	0.12	0.468	0.03
G-316*	800	50	30	15	4	n.d.	n.d.	n.d.
G-325*	800	50	30	30	4	n.d.	n.d.	n.d.
G-326*	800	50	30	50	5	n.d.	n.d.	n.d.
G-330*	800	50	30	10	4	n.d.	1.57 (33)	n.d.
MC-29	775	100	100	—	—	—	—	0.93
MC-18	775	100	75	21600	14	0.08	0.254 (37)	1.78
MC-21	775	100	75	10800	11	0.10	0.296 (53)	1.87
MC-23	775	100	75	3600	9	0.35	0.509 (71)	1.22
MC-28	775	100	75	60	6	1.93	3.193 (1814)	1.79
MC-34	775	100	75	10800	6	0.26	1.122 (672)	3.04
MC-38	775	100	75	1800	6	0.23	1.519 (70)	0.95
MC-39	775	100	75	3600	8	1.00	1.020 (18)	0.95
G-306	740	150	100	10	3	1.42	6.60 (59)	n.d.
G-311	740	150	100	20	3	2.03	5.01 (107)	n.d.
G-315	740	150	100	15	2	n.d.	n.d.	n.d.
G-329	740	150	100	30	2	n.d.	n.d.	n.d.
G-308	740	150	80	10	3	5.05	10.1 (11)	n.d.

[a] P_I = pressure of 3-d hydration; P_F = final pressure for quench; size = mean size of nucleated bubbles; BND = bubble number density; CND = crystal number density. All times are those held at lower pressure after pressure had dropped. The decrease in pressure occurred in 1–2 s for runs hydrated at 50 MPa, and in 2–4 s for all others. Run products are melt (quenched to glass) + bubbles + magnetite + hematite. Some samples also contain plagioclase, marked with*.

[b] Standard deviations for BND are listed in parentheses in units of the last digit of the BND; e.g., 0.675(177) should be read 0.675 ± 0.177.

follows solubility as expected (Fig. 2). We thus believe that the presence of $\sim 9 \times 10^{-6}$ moles of air in our runs had negligible effect on melt hydration.

Bubbles nucleated in our samples on faces of crystals, and as discussed below there are systematic variations of nucleation with number of crystals, degree of supersaturation, and water diffusivity. In addition, the number densities of bubbles nucleated in our runs are similar to those run at similar conditions by Hurwitz and Navon (1994), who used solid slabs of obsidian as their starting material, which hence would contain no air. We thus believe that the bubbles nucleated in our runs are filled with H_2O and not air.

Bubbles that nucleated after decompression are easily distinguished from hydration bubbles, because nucleated ones are <15 μm in size and much more numerous (Fig. 1). In this study, we report only the nucleated bubbles (Table 2). Hydration bubbles do have melt shells around them in which new bubbles did not nucleate, as has been seen before in similar experiments (Gardner et al., 1999, 2000; Larsen and Gardner, 2000). We focus on melt pools that are sufficiently far away from the hydration bubbles, such that the presence of the hydration bubbles had little effect.

Previous work showed that hydrating for 3 d is more than enough time for water to completely homogenize in rhyolitic melts (Gardner et al., 1999, 2000). Although we did not analyze our samples for dissolved H_2O contents, other work on MCR rhyolite has indeed found that 3 d are enough for homogenization (Fig. 2). In addition, because dissolved H_2O contents in hydrated MCR match those predicted from the water solubility solution of Gardner et al. (1999), we use that solution in this study to estimate dissolved H_2O contents. It should be noted, however, that the solubility curve was fitted to samples hydrated at 800–850°C, whereas some of our experiments ran at 740–775°C. Although lower temperatures produce higher dissolved H_2O contents, the differences are expected to be <0.1 wt% (Holtz et al., 1995). We have not corrected for temperature.

All experiments in this study were run at subliquidus condi-

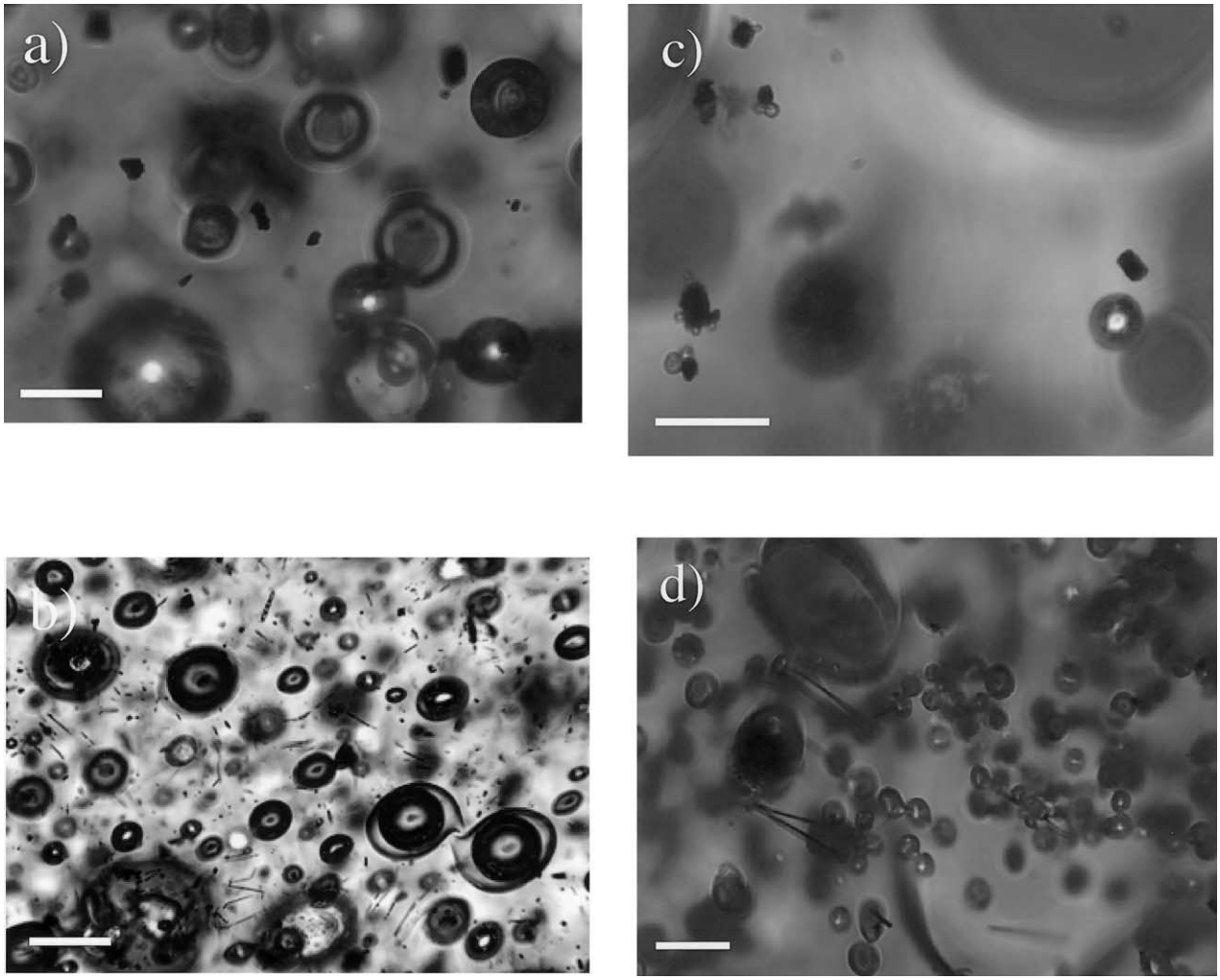

Fig. 1. Photomicrographs of experimental products (see Table 2 for run conditions). (a) MC-31 (P_I = 175 MPa, P_F = 175 MPa); scale bar = 20 μm. Note the presence of large hydration bubbles and only blocky-shaped Fe-Ti oxides. (b) MC-29 (P_I = 100 MPa, P_F = 100 MPa); scale bar = 50 μm. Fe-Ti oxides are both blocky and rod shaped. (c) MC-51 (P_I = 150 MPa, P_F = 125 MPa); scale bar = 10 μm. Relatively low supersaturation nucleated bubbles on blocky oxides. Note blocks seed multiple bubbles. (d) G-309 (P_I = 150 MPa, P_F = 80 MPa); scale bar = 10 μm. Relatively high supersaturation nucleated bubbles on both blocky oxides and at ends of rod-shaped oxides, but not along the lengths of the rods. (e) G-306 (P_I = 150 MPa, P_F = 100 MPa); scale bar = 10 μm. Low supersaturations at 740°C nucleated bubbles on at ends of rod-shaped oxides, but not along the lengths of the rods. (f) G-308 (P_I = 150 MPa, P_F = 80 MPa); scale bar = 10 μm. High supersaturations at 740°C nucleated bubbles along the full lengths of rod oxides.

tions, and crystallized Fe-Ti oxides ± plagioclase, depending on hydration pressure and temperature (Fig. 3). Crystals are dispersed relatively homogeneously throughout the samples, and did not grow in any alignment or zones, as was seen in Hurwitz and Navon (1994). Every sample contains Fe-Ti oxides to varying amounts, including runs that were not decompressed before quenching, and the amount of Fe-Ti oxides increases with lower temperature and hydration pressure. Those results show that they did not form because of the pressure drop.

Fe-Ti oxides are either blocky or needle-shaped. Blocky ones are ~0.5–5 μm in size and those large enough were identified with an electron microprobe as titano-magnetite, here after referred to as magnetite. Needle-shaped grains were too narrow to analyze with the microprobe, and thus we subjected three samples (G-304, G-306, and MC-49) to demagnetization experiments to identify them. MC-49 has only blocky magnetite, whereas the other two have magnetite and needle-shaped oxides. Each sample was first subjected to initial alternating field demagnetization in peak fields of 0.1 Tesla, followed by IRM acquisition in successively greater fields from 5 mT to 1 T, and then by alternating field demagnetization. All three were then given an IRM in a 1-T field and subjected to thermal demagnetization in 16 steps from 150 to 600°C. The alternating field demagnetization following near saturation IRM shows a clear magnetite signal for MC-49, with a very low to zero signal above 10 mT. In contrast, G-304 has a signal that persists to ~70 mT, whereas G-306 still has a signal above 100 mT, indicating that hematite is present in both. Thermal demagnetization curves give blocking temperatures that confirm the presence of magnetite in all three and hematite in the two.

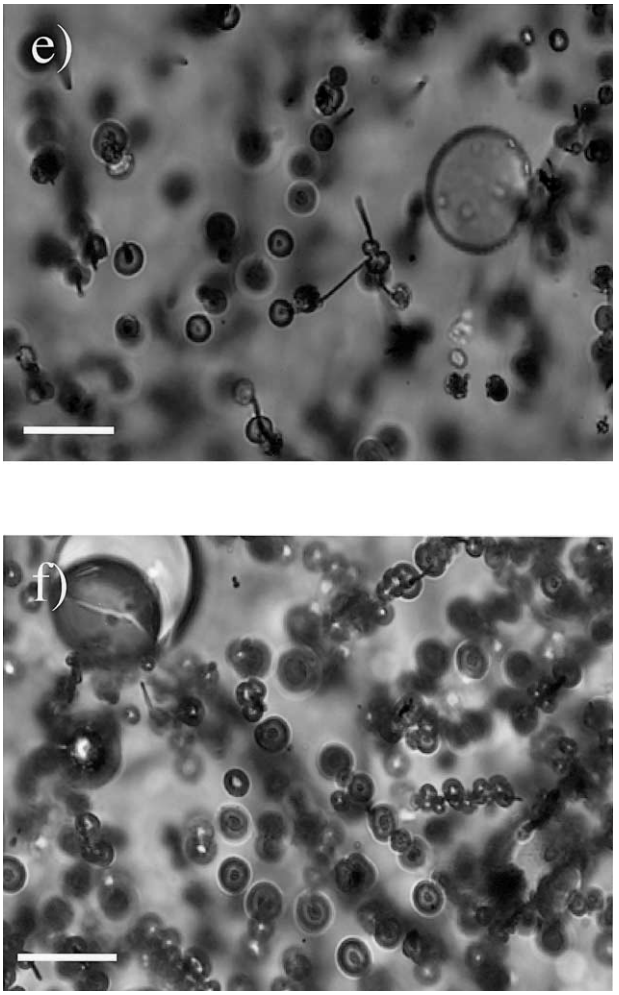

Fig. 1. (Continued)

Based on these results, we assume that all needle-shaped oxides in our samples are hematite.

Between 775–800°C, there are ~0.2 to 0.6 vol% oxide crystals, which change systematically in ratio of magnetite to hematite. At 175 MPa, almost all oxides are magnetite, whereas at 50 MPa they are mainly hematite. At 740°C, the number and amount of oxides increase dramatically to ~2 vol%, with most being hematite, although blocky magnetites occur. Hematite remains ~0.5 μm wide, but their lengths increased greatly from ~10–20 μm to ~10–55 μm with lower temperature and saturation pressure.

Only samples run at 800°C and 50 MPa contain plagioclase in addition to magnetite and hematite. Plagioclase is lath shaped, typically 5 to 10 μm long, and make up 1–2 vol% of the samples. Samples run at 740 and 775°C lack plagioclase, even though conditions were at the stability limit of plagioclase (Fig. 3). It is likely that running so close to the stability limit inhibited their growth (Lasaga, 1998).

When comparing hydration samples with those that underwent decompressions before being quenched, we find that only runs held at lower pressure for more than 3600 s are more crystalline than those quenched before decompression. In those longer duration runs oxides grew in abundance from ~0.2 to

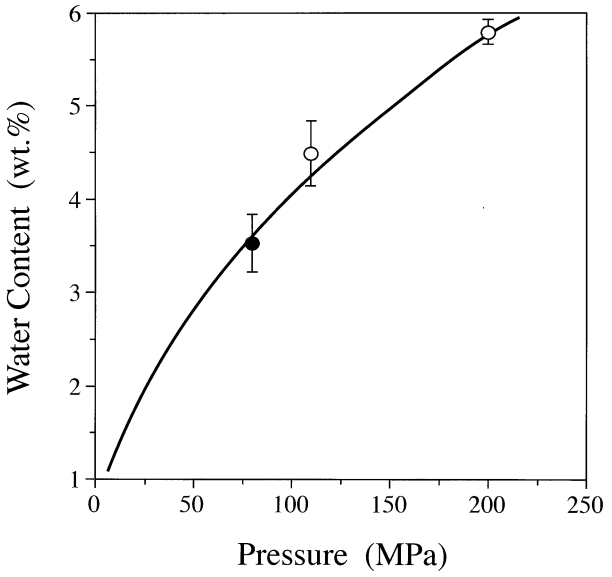

Fig. 2. Dissolved water contents in Mono Craters rhyolite experiments as a function of experimental pressure; open symbols for runs at 825°C and closed symbol at 875°C. Note that water contents follow the water solubility curve (dashed curve) fitted for rhyolitic melts at 800–850°C from Gardner et al. (1999). Water contents determined by Fourier-transform infrared spectroscopy (J. Larsen, unpublished data, 2003).

~0.6 vol%. Considering that most decompression runs were quenched much quicker than 3600 s (Table 2), we assume that the number of crystals did not change during the bubble nucleation period of our experiments. We also assume that the microlite contents of our samples are too small to affect melt composition and viscosity.

3.2. Decompression Experiments

In every decompressed sample, many small bubbles nucleated (Fig. 4)), and comprise 0.1 to 5 vol% of the samples (Table

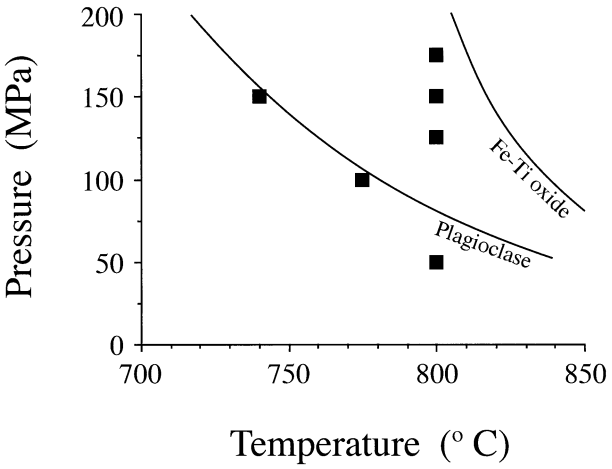

Fig. 3. Phase equilibrium diagram for Mono Craters rhyolite used in this study (Table 1). Curved lines mark the stability limits of Fe-Ti oxide and plagioclase (J. Larsen and M.-H. Denis, unpublished data, 2003). Filled squares show the conditions at which samples of this study were hydrated (Table 2).

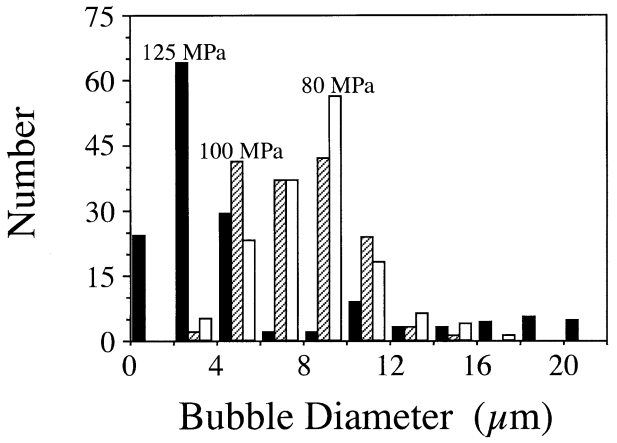

Fig. 4. Representative size distributions of nucleated bubbles. Samples were hydrated at 800°C and 150 MPa, decompressed to lower pressures (listed in figure), and held at lower pressure for 15 s (Table 2). Note that sizes increase with lower pressure. Samples shown are MC-51 (P_F = 125 MPa), G-314 (P_F = 100 MPa), and G-319 (P_F = 80 MPa).

2). Those bubbles are not seen in samples that were quenched without decompressing, and many are attached to crystal faces, suggesting that nucleation was heterogeneous in our experiments. In crystal-poor samples, many bubbles are not attached to visible crystals. Even in those runs, however, nucleation had to be heterogeneous because our decompressions are lower than those needed to nucleate bubbles homogeneously in rhyolitic melts (Navon and Lyakhovsky, 1998; Mourtada-Bonnefoi and Laporte, 1999; Mangan and Sisson, 2000). We note that N_T differs among samples run at the same decompression conditions and times (Table 2). Their differences are small, however, when compared to those between runs of differing decompressions and times. For example, the average N_T produced by decompressing from 150 to 100 MPa or from 125 to 105 MPa at 800°C is 7.5($\pm$1.3) $\times$ 10^7 and 3.8($\pm$0.7) $\times$ 10^7 cm^{-3}, respectively. We thus believe that our measured values of N_T represent nucleation at the experimental conditions. Overall, N_T ranges from 2 $\times$ 10^7 to 1 $\times$ 10^9 cm^{-3}, and increases as the amount of pressure drop increases, at a given hydration pressure and temperature (Table 2).

When specific bubbles nucleated can be determined from the change in numbers of bubbles in one run from those in a run of shorter duration. For example, the change in the numbers of bubbles between 25 and 35 s following a 100 MPa decompression from 150 MPa (at 800°C) is the numbers of bubbles of various sizes in G-299 minus those in G-307 (Fig. 5). In this case, bubbles smaller than 8 μm decreased in number between 25 and 35 s, whereas larger ones became more numerous, showing that no bubble $<8\mu$m appeared between 25 and 35 s. Note that to compare samples, the total number of bubbles counted must equal or be normalized. Examining changes in bubble populations shows that almost all bubbles nucleated in less than 10 s for all decompression conditions (Fig. 6). Most new bubbles are <15 μm in size, although those in 740°C experiments are generally smaller and more restricted in size. A few 2–3 μm-sized bubbles appear after 15 s, but are too few to increase N_T. In fact, N_T decreases by more than an order of magnitude as hold time increases to 6 h, showing that no more significant nucleation occurred (Fig. 7). In addition to a decrease in N_T, small bubbles decrease in number, and larger ones increase, with hold time, suggesting that bubbles grew and coalesced with time.

Magnetite seed bubbles in all experiments. When ΔP = 20–25 MPa, magnetite seeded one to a few bubbles, depending on crystal size (Fig. 1). At ΔP = 50–70 MPa, many bubbles are attached to magnetite, and often completely surround grains. Nucleation on hematite varied greatly with supersaturation and temperature. In the 800°C runs, hematite seeded no bubbles (extremely rarely only one) at 20–25 MPa drops, whereas at 50–70 MPa drops hematite seeded bubbles, but mainly on their ends. Rarely did bubbles nucleate along the

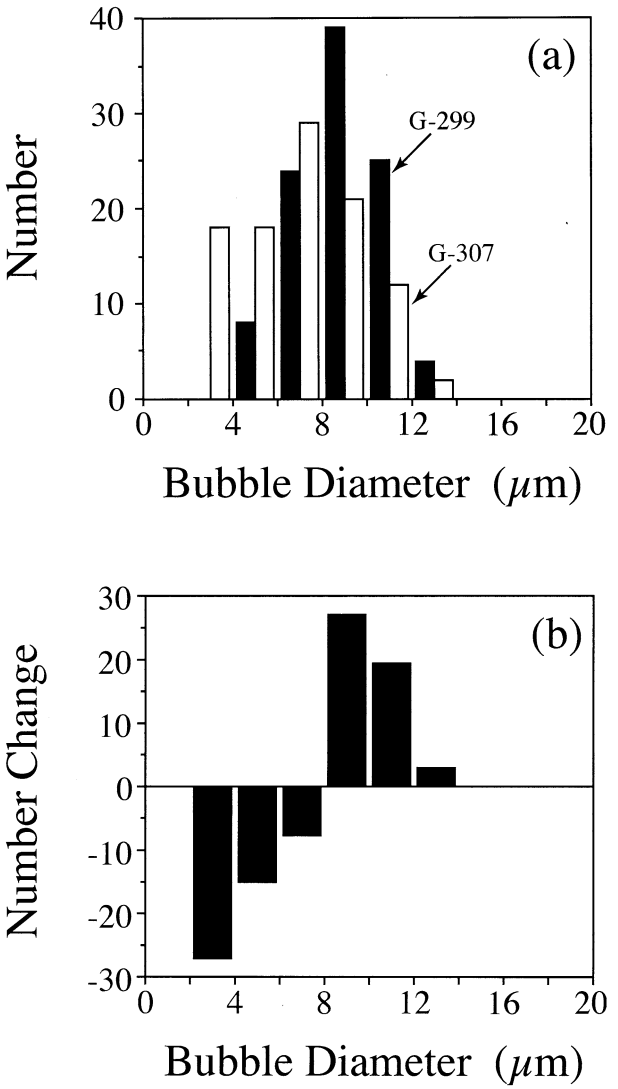

Fig. 5. (a) Bubble size distributions in two samples that hydrated at the same conditions and underwent the same decompression, but were held at lower pressure for either 25 s (G-307) or 35 s (G-299) (Table 2). The changes with time of bubbles of each size are shown in (b). Note that the number of bubbles <8 μm decrease with time, whereas larger ones become more numerous, and hence no new bubbles nucleated during the 10-s interval. To calculate such changes, the total number of bubbles counted must be the same or normalized.

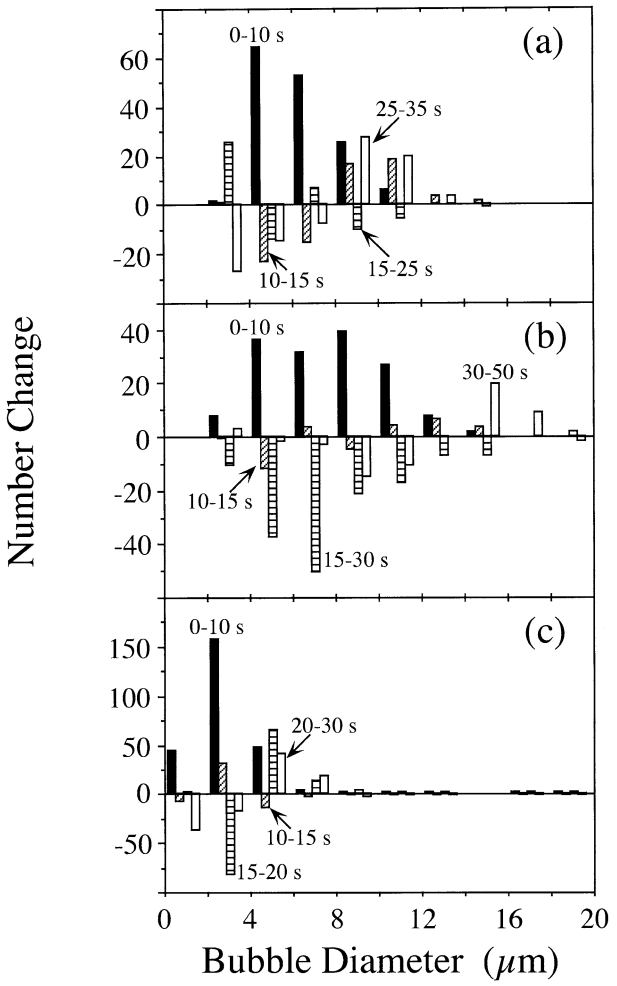

Fig. 6. Differences in bubble size distributions as a function of time in (a) samples hydrated at 800°C and 150 MPa and decompressed by 50 MPa, (b) samples hydrated at 800°C and 50 MPa and decompressed by 20 MPa, and (c) samples hydrated at 740°C and 150 MPa and decompressed by 50 MPa. See Figure 5 for discussion of calculations.

long surfaces of hematite. At 740°C, bubbles nucleated on any magnetite present, and on the ends of hematite needles when the pressure drop was 50 MPa. When pressure dropped by 70 MPa, however, many bubbles nucleated along the entire lengths of hematite, forming long chains of bubbles (Fig. 1). Although plagioclase microlites are present at 800°C and 50 MPa, no bubbles are attached to their faces.

4. DISCUSSION

4.1. Nucleation of Heterogeneous Bubbles

A new population of 2×10^7 to 1×10^9 cm^{-3} bubbles nucleated in less than 10 s. Given that almost all bubbles nucleated faster than our quickest quench, it is impossible to directly estimate bubble nucleation rates. At the very least, however, nucleation rates exceeded 2×10^6 to 1×10^8 cm^{-3} s^{-1}, given N_T at 10 s. Such rates compare with those of Hurwitz and Navon (1994), who found heterogeneous nucleation rates $>10^6$ cm^{-3} s^{-1}. It must be stressed that the above rates are minima.

It is unlikely that the observed sizes of bubbles are the critical size of nuclei, as the critical size of a H_2O bubble nucleus is <1 μm (Mangan and Sisson, 2000). Instead, the sizes in our experiments probably reflect some growth of the bubbles after they nucleated, mostly as a result of water diffusing from the surrounding melt shells of the nuclei (see Section 4.4).

Bubbles nucleated at 740°C are mostly smaller (1–5 μm) than those nucleated at higher temperatures (Fig. 6). That difference occurred despite equal ΔP, arguing that the smaller sizes resulted from their greater numbers. A certain amount of ΔP means that a given mass of H_2O becomes available to form bubbles. If that H_2O must be distributed between many bubbles, then their sizes will naturally be smaller than if few bubbles compete for H_2O. The greater lengths of hematite needles allowed many more closely spaced nuclei to form at 740°C, which then grew to smaller sized bubbles.

A few new bubbles appear in our samples after 15 s (Fig. 6). Pressure drops are too small for them to have nucleated homogeneously. Instead, their appearance indicates either that some small amount of heterogeneous nucleation occurred over longer time spans, that some bubbles may simply have needed more time to grow large enough to be seen, or that growth of some bubbles delayed the appearance of others (Larsen and Gardner, 2000). It is unclear which scenario better explains their appearance.

4.2. Influence of Crystals on Bubble Nucleation

At equal values of ΔP, N_T is 2–10 times greater at 740°C than at 800°C. Magnetite and hematite microlites are more abundant at lower temperature, and thus an increased number of oxide crystals increased bubble nucleation. In addition, more bubbles are seeded per crystal as ΔP increased. At the highest

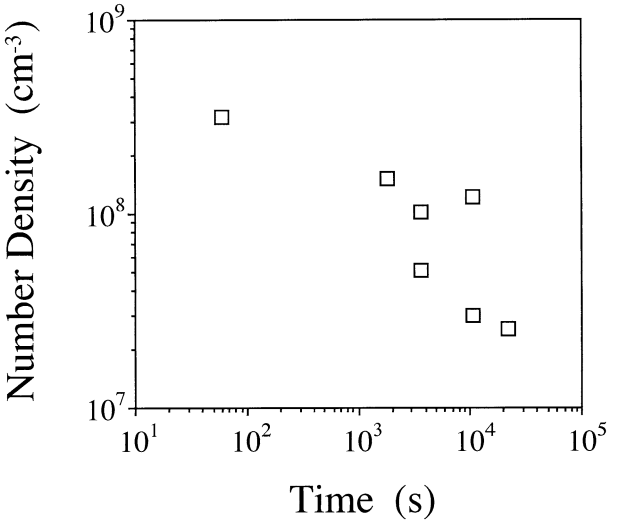

Fig. 7. Variations in bubble number density as a function of time held at lower pressure for long periods of time (Table 2). Note that number density decreases with time, indicating that no nucleation occurred beyond ~1 h.

values of ΔP, each magnetite typically seeded several bubbles and hematites seed many bubbles along their entire lengths (Fig. 1). This indicates that not only an increase in abundance of Fe-Ti oxides leads to greater nucleation, but also that more sites on those crystals can be active for nucleation.

We cannot measure accurately the wetting angles of bubbles on either magnetites or hematites, but we caution that any visible angle is unlikely to be a critical wetting angle. This is because nucleation in most samples stopped because bubbles grew (see Section 4.4). That growth would modify the angle between the bubble and crystal. Hurwitz and Navon (1994) were unable to match observed angles with those expected from their bubble number densities, and it may be likely that growth had also modified bubble sizes in their runs.

Nucleation on hematite varied as a function of ΔP. One reason may be that roughness varies on the crystals, as a corner allows heterogeneous nucleation at a significantly lower ΔP relative to a flat surface (Hurwitz and Navon, 1994). This may explain why bubbles nucleated at the ends of the hematite at lower ΔP compared to their sides. Alternatively, there may be a structural change between faces on hematite that leads to variable σ_{cv} with location on the crystal. Different wetting angles result from different σ_{cv} (Eqn. 3). We can estimate the difference in σ_{cv} by assuming that homogeneous nucleation would occur in our melts at 120 MPa (i.e., $\sigma_{mv} = 0.1$ N m^{-1}), that the critical values of ΔP for nucleation at the ends and on lengths of hematite are 50 and 70 MPa, respectively, and that both sites are flat. Using the derived relationship between θ and reduced supersaturation pressure needed for nucleation from Hurwitz and Navon (1994), then the difference in σ_{cv} between the two hematite sites is ~0.033 N m^{-1}, meaning that σ_{cv} at the ends of hematite is 0.033 N m^{-1} lower than that on their lengths. That difference is approximately constant for all changes in our assumptions about homogeneous ΔP (except when it approaches 70 MPa) and its related variation in σ_{mv} (Hurwitz and Navon, 1994). If homogeneous $\Delta P = 70$ MPa, then the difference in σ_{cv} becomes ~0.059 N m^{-1}. These are only rough estimates, and more work is needed to address why nucleation on hematite varied.

Plagioclase did not seed bubbles. Although our highest ΔP for plagioclase-bearing samples was 20 MPa, this represents ~31% supersaturation of H_2O in the melt (equal to ΔP of ~60 MPa from 150 MPa). That is a significant supersaturation, suggesting that the σ_{cv} for plagioclase-H_2O is relatively high, certainly greater than those of magnetite and hematite. Hurwitz and Navon (1994) were also unable to nucleate bubbles on plagioclase even at $\Delta P = 134$ MPa, even though they estimated that homogeneous nucleation should have occurred at ~60 MPa. Although more work is needed to find when plagioclase can seed bubbles, these results suggest that the σ for plagioclase-H_2O may exceed that for rhyolitic melt-H_2O.

Finally, not all nucleation occurred on crystals, as some bubbles have no visible crystals attached. Those bubbles must have nucleated on some type of submicroscopic heterogeneity in the melt. Hurwitz and Navon (1994) found similar results, and argued that those sites are probably incompletely melted crystals left over from hydrating the melt. It is likely that our samples contain similar heterogeneities.

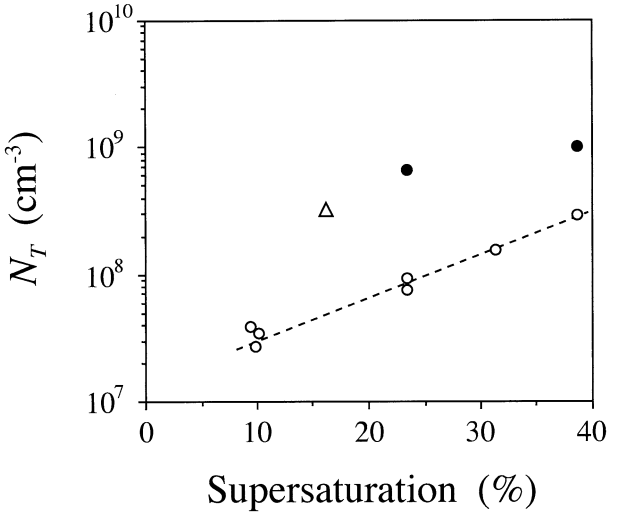

Fig. 8. Variations in N_T as a function of degree of supersaturation. Data shown are samples quenched 10–15 s after decompression, except MC-28 (60 s). Symbols are for different temperatures: open circles = 800°C; triangle = 775°C; filled circles = 740°C. Dotted line is an exponential fit ($r = 0.998$) to the 800°C data. Note that at equal supersaturations, there is an order of magnitude increase in N_T between 800°C and colder samples, because of the increased number of Fe-Ti oxides.

4.3. Influence of Supersaturation on Bubble Nucleation

Lower pressure supersaturates melts with respect to H_2O, but a given amount of pressure drop can equal different degrees of supersaturation, because H_2O solubility is nonlinear with pressure (Fig. 2). To convert our pressure drops to supersaturations, we estimated the H_2O contents expected at the starting and ending pressures of each run from solubility (Fig. 2), and express the excess H_2O as a percentage of the final H_2O content. For example, solubility predicts H_2O contents of 4.94 and 4.01 wt% at 150 MPa and 100 MPa, respectively, and so a sample hydrated at 150 MPa and then decompressed to 100 MPa will be 23.2% supersaturated. We calculated supersaturations for samples quenched 10–15 s after pressure had dropped to determine the influence of supersaturation pressure on N_T (Fig. 8). We also include sample MC-28, assuming that N_T did not change between 10 and 60 s. At 800°C, an increase in supersaturation from 9.5 to 38.6% resulted in an exponential increase in N_T (correlation coefficient = 0.998). Fewer results exist for samples at 740°C, but greater supersaturations did produce greater N_T. Importantly, we find that N_T increases with supersaturation in samples hydrated at 800°C and 150 MPa, and thus all have very similar amounts and numbers of crystals. Our results thus indicate that the degree of supersaturation influences heterogeneous nucleation of bubbles. The elevated values of N_T between the 740 and 800°C samples most likely result from the greater abundance of crystals.

From Eqn. 1, it can be seen that for both homogeneous and heterogeneous nucleation, the activation energy for nucleation increases with greater supersaturation, thus allowing more nuclei to form. In homogeneous nucleation, this occurs mainly by decreasing the critical size of a stable nucleus (Lasaga, 1998). For heterogeneous nucleation, increased supersaturation will

not only decrease critical size, but probably also allow more sites to be utilized. It should be noted that on flat surfaces, the reduction in ΔP for heterogeneous relative to homogeneous nucleation does not exceed 50% until θ exceeds ~110°. Increasing supersaturation forces more H_2O molecules to cluster together, and if they do this along the surface, then they will form at a greater θ, and all contacts that form wetting angles $\geq\theta$ can be nucleation sites. This may explain why each magnetite can seed greater numbers of bubbles as ΔP increases.

4.4. Influence of Bubble Growth on Nucleation

When bubbles grow they deplete the melt with respect to H_2O, and thus decrease any supersaturation available for nucleation (Toramaru, 1989, 1995). Bubbles grow faster as water diffusivity increases (Proussevitch et al., 1993; Proussevitch and Sahagian, 1998), and thus fewer bubbles should nucleate with greater diffusivity (Toramaru, 1989, 1995). Growth is hindered by high melt viscosity, which in turn would allow the melt to remain supersaturated longer, and hence more bubbles can nucleate. Viscosity and diffusivity are linked, however, as greater H_2O contents and higher temperature increase diffusion but decrease viscosity (Shaw, 1972; Jambon, 1979; Delaney and Karsten, 1981; Zhang et al., 1991; Hess and Dingwell, 1996; Zhang and Behrens, 2000).

Toramaru (1995) proposed that N_T varies proportionally with either one of two scales, depending on whether nucleation is influenced by H_2O diffusion or melt viscosity. When diffusion dominates, N_T is expected to vary as a function of the dimensionless parameter α_3, which is defined as

$$\alpha_3 = \frac{RT\frac{C_o}{P_o}DP_o}{\lambda r_o^2} \quad (6)$$

where $RT(C_o/P_o)$ is the volume fraction of initial gas concentration, C_O, (number m^{-3}) at temperature T (K) and initial pressure P_O, with R being the gas constant (J k^{-1}), D is water diffusivity (m^2 s^{-1}), λ is decompression rate (Pa s^{-1}), and r_O is a scaling constant of bubble radius ($=2\sigma/P_o$). When viscosity dominates, ln n (where $n = 2\ N_T\ C_O^{-1}$) is expected to be proportional to the dimensionless parameter α_4, which is defined as

$$\alpha_4 = \frac{P_o^2}{4\mu\lambda} \quad (7)$$

where μ is viscosity (Pa s). The transition from the diffusion-controlled to the viscosity-controlled regimes is expected to occur at $\alpha_4 < 2000$ (Toramaru, 1995).

The influence of bubble growth on nucleation can thus be evaluated by examining the variation of N_T (or n) with α_3 or α_4. To evaluate growth in our experiments, we focus on runs quenched 10–15 s after decompressing, because all nucleation occurred in the first 10 s. Values of α_3 and α_4 were determined by assuming that $\sigma = 0.11$ N m^{-1}. Although σ likely varies with H_2O content (Epel'baum et al., 1973; Bagdassarov et al., 2000), its variation is too poorly known at this time to allow a fuller analysis. We use the models of Zhang and Behrens (2000) and Hess and Dingwell (1996) to estimate D and μ, respectively. Values for D vary between ~4×10^{-12} and ~8×10^{-12} m^2 s^{-1}, whereas μ varies between ~4×10^4 and ~5×10^5 Pa s.

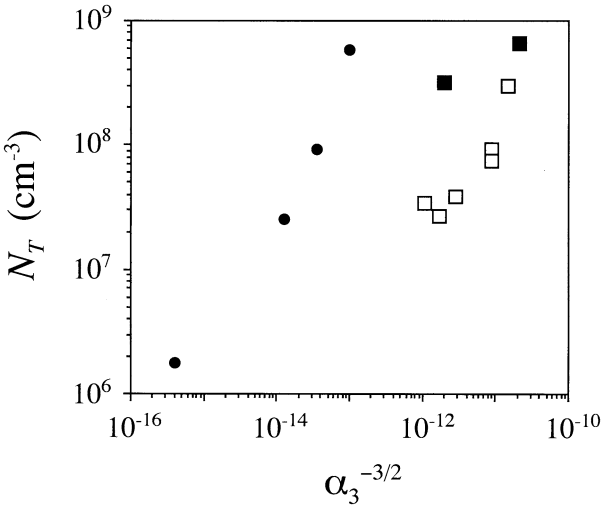

Fig. 9. Variations in N_T as a function of the parameter $\alpha_3^{-3/2}$ (see Eqn. 6). Data shown are samples with $\alpha_4 > 2000$ and quenched 10–15 s after decompression, except MC-28 (60 s). Open squares = 800°C samples, filled squares = 775 and 740°C (G-306) samples. Also shown as filled circles are data from Gardner et al. (1999). Note that N_T generally increases for the different series with increasing $\alpha_3^{-3/2}$, as is expected if water diffusion regulates nucleation (Toramaru, 1995).

Most of our experiments were run at conditions such that $\alpha_4 > 2000$ (~2800–96,000), and so water diffusion should have played a significant role in nucleation, and if so we should find that $N_T\ \alpha\ (\alpha_3)^{-1.5}$, as predicted by Toramaru (1995). In fact, we find a relatively strong log linear correlation between N_T and $(\alpha_3)^{-1.5}$ (Fig. 9). We note, however, that α_3 is a function of both D and λ. Unfortunately, those both vary between our runs, and so we cannot isolate either factor. In a similar study, however, Gardner et al. (1999) hydrated rhyolitic melts at 200 MPa and 825°C, and hence D was the same among runs, and decompressed them at different λ. There is in fact a strongly linear trend between N_T and $(\alpha_3)^{-1.5}$ (Fig. 9). These results show that nucleation can be influenced by bubble growth, and that the magnitude of that influence relates to D and λ.

Only two samples were viscous enough such that $\alpha_4 \leq 2000$, and so we cannot fully evaluate the influence of viscosity on heterogeneous nucleation. Between those two, however, N_T decreases slightly as α_4 decreases from ~2000 to ~625 (Fig. 10). Such a change in α_4 should correspond to a ~500-time increase in N_T, contrary to our results. In a similar study, Gardner et al. (2000) decompressed highly viscous, water-saturated rhyolitic melts (α_4 = ~8–2000), and found that at λ = 0.25 MPa s^{-1}, bubbles nucleated heterogeneously at $\mu \leq 10^8$ Pa s, but not at $\mu = 10^{8.8}$ Pa s. At λ = 0.125 MPa s^{-1}, bubbles nucleated even when $\mu = 10^{8.8}$ Pa s. Despite the generally lower values of α_4, however, n values of those runs are lower than those of this study, including no nucleation at α_4 = 8 (Fig. 10). We note that a change in α_4 from ~2000 to 8 should correspond to eight orders of magnitude increase in N_T, and not to a general decrease. A lower n with lower α_4 is not expected if viscosity simply hinders growth, and allows more bubbles to nucleate. Instead, viscosity may not only hinder

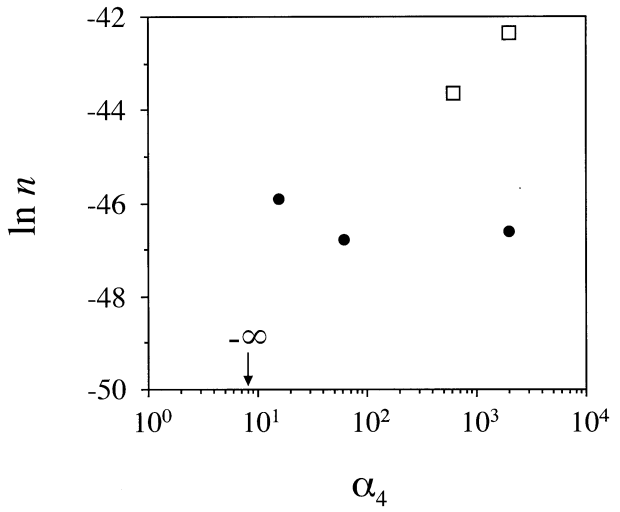

Fig. 10. Variations in ln n as a function of the parameter α_4 (see Eqn. 7). Only G-308 and G-330 (open squares) are shown as they have $\alpha_4 \leq 2000$ and were quenched 10–15 s after decompression. Also shown as filled circles are data from Gardner et al. (2000); note that one sample ($\alpha_4 = 7.8$) did not nucleate bubbles and hence ln $n = -\infty$. In general, ln n decreases as α_4 decreases, opposite of that expected if melt viscosity limits growth and, hence, increases nucleation (Toramaru, 1995).

bubble growth (Navon et al., 1998; Gardner et al., 2000), but also suppress nucleation.

Finally, whether bubble growth influences bubble nucleation through D or μ, both regimes result in a single, short-lived nucleation event (Toramaru, 1989, 1995). Indeed, we found that almost all bubbles nucleated in our experiments in less than 10 s. Martel and Bureau (2001) also found a single nucleation event occurred during unsteady decompressions from high pressures (700–2190 MPa).

4.5. Implications for Magmatic Degassing and Volcanic Eruptions

Our results show that if H_2O-saturated magma contains heterogeneities, then 10^7-10^9 cm^{-3} bubbles can nucleate in less than 10 s, with the number of bubbles depending on the number of sites and supersaturations. Magmas can nucleate bubbles during storage at depth, as shown by the 1991 eruption of Pinatubo volcano and the Bishop Tuff eruption of Long Valley Caldera, which both tapped magmas that contained bubbles at depth (Westrich and Gerlach, 1992; Wallace and Gerlach, 1994; Wallace et al., 1999). Taking our water solubility (Fig. 2) and assuming that water behaves incompatibly, we find that if a magma is already saturated with H_2O, then it need crystallize only ~0.2–4% more to generate an over-pressure of 1 MPa, with the greater crystallization needed at very low pressures (10 MPa). Thus, once magma is H_2O saturated, it need crystallize only a small amount to form a gas phase. Nucleating bubbles at depth has been proposed as a trigger for volcanic eruptions (Blake, 1984; Tait et al., 1989; Pyle and Pyle, 1995).

Comparable number densities are not produced by homogeneous nucleation until ΔP >120–170 MPa (Hurwitz and Navon, 1994; Mourtada-Bonnefoi and Laporte, 1999; Mangan and Sisson, 2000). It is important to note that such supersaturations equal or exceed the total H_2O pressures of many erupted magmas (e.g., Rutherford et al., 1985; Gardner et al., 1995, 2002; Cottrell et al., 1999). For erupting magmas to nucleate bubbles homogeneously, they must have water contents greater than ~4.4–5.3 wt% (H_2O saturation at 120–170 MPa). In addition, it is unlikely that magma can supersaturate by 120–170 MPa while stored at depth, because the walls of a shallow level magma chamber would fail from over-pressures on order of 20 MPa (Tait et al., 1989).

A potentially surprising finding is that high melt viscosities may limit the ability of bubbles to nucleate, contrary to that expected if the only effect of viscosity was to prevent bubble growth (Toramaru, 1995). Nucleation was not completely inhibited, however, until $\mu \sim 10^9$ Pa s, and only at relatively high decompression rates. As pointed out by Gardner et al. (2000), such high viscosities are not reached in rhyolitic melts except at very low temperatures or very low water contents. It is thus unlikely that nucleation is completely suppressed by viscosity, except possibly in a cooling surface dome.

5. CONCLUSIONS

Heterogeneous bubble nucleation has been examined by experimentally hydrating rhyolitic melts at subliquidus conditions. Between 2×10^7 and 1×10^9 cm^{-3} bubbles nucleated on crystal faces of magnetite and hematite, essentially all within 10 s. Our results reveal important influences on nucleation:

- Increased numbers of Fe-Ti oxide crystals increase the density of bubbles
- Nucleation varied as a function of position on hematite as ΔP changed, from either variable surface roughness or a change in σ_{cv} of ~0.03–0.05 N m^{-1} with position
- Increased degree of supersaturation increases the density of bubbles nucleated by activating more sites on crystals
- Decreasing water diffusivity and increasing decompression rate increase the density of bubbles nucleated by decreasing the amount of bubble growth
- High melt viscosity may inhibit bubble nucleation

A major difference between heterogeneous and homogeneous nucleation is the degree of supersaturation needed to induce bubbles to nucleate. Given that difference, it is likely that bubbles can only nucleate heterogeneously while magma is stored at depth. This is important if volcanic eruptions are triggered by the formation of gas phase.

Acknowledgments—This project was funded by a grant from the U.S. National Science Foundation (EAR-0087853) and carried out during a 6-month visit by M.-H. Denis to the Geophysical Institute during her second year in the "Magistère des Science Sciences de la Terre" program at the Ecole Normale Superiéure, Paris, France. The authors wish to thank Jessica Larsen for the Mono Craters obsidian sample and use of her unpublished data on the phase equilibrium of Mono Craters rhyolite. The authors also thank Dr. David Stone for performing the magnetization experiments that positively identified magnetite and hematite. The manuscript was improved greatly by reviews from Alex Proussevitch, Kelly Russell, C.C. Mourtada-Bonnefoi, Caroline Martel, Cliff Shaw, and an anonymous reviewer.

Associate editor: J. K. Russell

REFERENCES

Bagdassarov N., Dorfman A., and Dingwell D. B. (2000) Effect of alkalis, phosphorus, and water on the surface tension of haplogranite melt. *Am. Mineral.* **85,** 33–40.

Blake S. (1984) Volatile oversaturation during the evolution of silicic magma chambers as an eruption trigger. *J. Geophys. Res.* **89,** 8237–8244.

COESA. (1976) U.S. Standard Atmosphere. U.S. Printing Office.

Cottrell E., Gardner J. E., and Rutherford M. J. (1999) Dynamic movement and changing storage conditions of large silicic magma bodies: Evidence from the Minoan rhyodacite, Santorini, Greece. *Contrib. Mineral. Petrol.* **135,** 315–331.

Delaney J. R. and Karsten J. L. (1981) Ion microprobe studies of water in silicate melts: Concentration-dependent diffusion in obsidian. *Earth Planet. Sci. Lett.* **52,** 191–202.

Dobson P. F., Epstein S., and Stolper E. M. (1989) Hydrogen isotope fractionation between coexisting vapor and silicate glasses and melts at low pressure. *Geochim. Cosmochim. Acta* **53,** 2723–2730.

Epel'baum M. B., Bababashov I. V., and Salova T. P. (1973) Surface tension of felsic magmatic melts at high temperatures and pressures. *Geokhimiya* **3,** 461–464.

Gardner J. E., Rutherford M., Carey S., and Sigurdsson H. (1995) Experimental constraints on pre-eruptive water contents and changing magma storage prior to explosive eruptions of Mount St. Helens volcano. *Bull. Volcanol.* **57,** 1–17.

Gardner J. E., Hilton M., and Carroll M. R. (1999) Experimental constraints on degassing of magma: Isothermal bubble growth during continuous decompression from high pressure. *Earth Planet. Sci. Lett.* **168,** 201–218.

Gardner J. E., Hilton M., and Carroll M. R. (2000) Bubble growth in highly viscous silicate melts during continuous decompression from high pressure. *Geochim. Cosmos. Acta* **64,** 1473–1483.

Gardner J. E., Layer P. W., and Rutherford M. J. (2002) Phenocrysts versus xenocrysts in the Toba Tuff: Implications for the petrogenesis of 2800 km^3 of magma. *Geology* **30,** 347–350.

Geschwind C.-H. and Rutherford M. J. (1992) Cummingtonite and the evolution of the Mount St. Helens magma system: An experimental study. *Geology* **20,** 1011–1014.

Gray N. H. (1970) Crystal growth and nucleation in two large diabase dikes. *Can. J. Earth Sci.* **7,** 366–375.

Hess K.-U. and Dingwell D. B. (1996) Viscosities of hydrous leucogranitic melts: A non-Arrenian model. *Am. Mineral.* **81,** 1297–1300.

Holtz F., Behrens H., Dingwell D. B., and Johannes W. (1995) H_2O solubility in haplogranitic melts: Compositional, pressure, and temperature dependence. *Am. Mineral.* **80,** 94–108.

Hurwitz S. and Navon O. (1994) Bubble nucleation in rhyolite melts: Experiments at high pressure, temperature, and water content. *Earth Planet. Sci. Lett.* **122,** 267–280.

Jambon A. (1979) Diffusion of water in a granitic melt: An experimental study. *Carnegie Inst. Wash. Yrbk.* **78,** 352–355.

Larsen J. F. and Gardner J. E. (2000) Experimental constraints on bubble interactions in rhyolitic melts: Implications for vesicle size distributions. *Earth Planet. Sci. Lett.* **180,** 201–214.

Lasaga A. C. (1998) Kinetic Theory in the Earth Sciences. Princeton University Press.

Liu Y. and Zhang Y. (2000) Bubble growth in rhyolitic melt. *Earth Planet. Sci. Lett.* **181,** 251–264.

Mangan M. and Sisson T. (2000) Delayed, disequilibrium degassing in rhyolite magma. Decompression experiments and implications for explosive volcanism. *Earth Planet. Sci. Lett.* **183,** 441–455.

Martel C. and Bureau H. (2001) In situ high-pressure and high temperature bubble growth in silicic melts. *Earth Planet. Sci. Lett.* **191,** 115–127.

Mourtada-Bonnefoi C. C. and Laporte D. (1999) Experimental study of homogeneous bubble nucleation in rhyolitic magmas. *Geophys. Res Lett.* **26,** 3505–3508.

Mourtada-Bonnefoi C. C. and Laporte D. (2002) Homogeneous bubble nucleation in rhyolitic magmas: An experimental study of the effect of H_2O and CO_2. *J. Geophys. Res.* **107,** B4 10.1029/2001JB000290.

Navon O. and Lyakhovsky V. (1998) Vesiculation processes in silicic magmas. In *The Physics of Explosive Volcanic Eruptions* (eds. J. S. Gilbert and R. S. J. Sparks), pp. 27–50. Geol. Soc. Lond. Spec. Pub. 145.

Navon O., Chekhmir A., and Lyakhovsky V. (1998) Bubble growth in highly viscous melts: Theory, experiments, and autoexplosivity of dome lavas. *Earth Planet. Sci. Lett.* **160,** 763–776.

Proussevitch A. A., Sahagian D. L., and Anderson A. T. (1993) Dynamics of diffusive bubble growth in magmas: Isothermal case. *J. Geophys. Res.* **98,** 22283–22307.

Proussevitch A. A. and Sahagian D. L. (1998) Dynamics and energetics of bubble growth in magmas: Analytical formulation and numerical modeling. *J. Geophys. Res.* **103,** 18223–18251.

Pyle D. M. and Pyle D. L. (1995) Bubble migration and the initiation of volcanic eruptions. *J. Volcanol. Geotherm. Res.* **67,** 227–232.

Rutherford M. J., Sigurdsson H., Carey S., and Davis A. (1985) The May 18, 1980, eruption of Mount St. Helens, 1—Melt composition and experimental phase equilibria. *J. Geophys. Res.* **90,** 2929–2947.

Sato H. (1995) Textural difference between pahoehoe and aa lavas of Izu-Oshima volcano, Japan: An experimental study on population density of plagioclase. *J. Volcanol. Geotherm. Res.* **66,** 101–113.

Shaw H. R. (1972) Viscosities of magmatic silicate liquids: An empirical method of prediction. *Am. J. Sci.* **272,** 870–893.

Sparks R. S. J. (1978) The dynamics of bubble formation and growth in magmas: A review and analysis. *J. Volcanol. Geotherm. Res.* **3,** 1–37.

Tait S., Jaupart C., and Vergniolle S. (1989) Pressure, gas content and eruption periodicity of a shallow crystallizing magma chamber. *Earth Planet. Sci. Lett.* **92,** 107–123.

Toramaru A. (1989) Vesiculation process and bubble size distributions in ascending magmas with constant velocities. *J. Geophys. Res.* **9,** 17523–17542.

Toramaru A. (1995) Numerical study of nucleation and growth of bubbles in viscous magmas. *J. Geophys. Res.* **100,** 1913–1931.

Wallace P. J. and Gerlach T. M. (1994) Magmatic vapor source for sulfur dioxide released during volcanic eruptions: Evidence from Mount Pinatubo. *Science* **265,** 497–499.

Wallace P. J., Anderson A. T., Jr., and Davis A. M. (1999) Gradients in H_2O, CO_2, and exsolved gas in a large-volume silicic magma system: Interpreting the record preserved in melt inclusions from the Bishop Tuff. *J. Geophys. Res.* **104,** 20097–20122.

Westrich H. R. and Gerlach T. M. (1992) Magmatic gas source for the stratospheric SO_2 cloud from the June 15, 1991, eruption of Mount Pinatubo. *Geology* **20,** 867–870.

Zhang Y., Stolper E. M., and Wasserburg G. J. (1991) Diffusion of water in rhyolitic glasses. *Geochim. Cosmochim. Acta* **55,** 441–456.

Zhang Y. and Behrens H. (2000) H_2O diffusion in rhyolitic melts and glasses. *Chem. Geol.* **169,** 243–262.